FAST SURFACE DETECTION USING SINGLE-PHOTON DETECTION EVENTS

Abderrahim Halimi, Andrew Wallace, Gerald S. Buller, Stephen McLaughlin,

School of Engineering and Physical Sciences, Heriot-Watt University, Edinburgh U.K.

ABSTRACT

This paper presents a fast object detection algorithm for 3D single-photon Lidar data. Lidar imaging acquires time-of-flight (ToFs) events in different spatial locations to build a 3D image of the observed objects. However, high ambient light or obscurants, might affect the reconstruction quality of the 3D scene. This paper proposes a solution by first detecting the pixels containing photons reflected from a object/surface, allowing a higher level processing of the data while only accounting for informative pixels. In contrast to histogram based approaches, the proposed algorithm operates on the detected photon events allowing a reduction in memory requirements and computational times. A Bayesian approach is considered leading to analytical estimates that can be computed efficiently. Results on simulated and real data highlight the benefit of the proposed approach when compared to a state-of-the-art algorithm based on histogram of counts.

Index Terms— 3D Lidar imaging, Bayesian approach, target detection, sparse photon regime, single-photon events.

1. INTRODUCTION

Single-photon 3D laser detection and ranging (Lidar) imaging has emerged as a candidate technology for a number of application areas including defence, automotive [1], and environmental sciences [2]. This imaging system builds a high-resolution 3D image of the observed objects by sending laser pulses and collecting the reflected photons from a surface while measuring their time-of-flight (ToFs). The ToFs contain information about the system-target distance while the number of collected photons inform on the reflectivity of the observed scene. It is also common to pre-process the detected ToFs events into a histogram of counts and to apply different processing strategies on the resulting waveforms. However, this data representation is memory inefficient especially in the sparse photon regime, and requires an additional computational cost to convert photon events to histograms. This paper operates on the raw ToFs photon events to ensure an optimized exploitation of the available computational resources.

This work was supported by the UK Royal Academy of Engineering under the Research Fellowship Scheme (RF/201718/17128), EPSRC Grants EP/T00097X/1,EP/S000631/1,EP/S026428/1,EP/N003446/1, the Dasa project DSTLX1000147844 and the MOD University Defence Research Collaboration (UDRC) in Signal Processing.

Thanks to their good resolution and low sensitivity to noise, time-correlated single-photon counting (TCSPC) Lidar systems are currently used to perform long-range imaging [3] in addition to imaging through obscurants [4–7]. Several pixels are scanned in both cases, however, some pixels might only contain background counts due to ambient light, reflection from the observation environment (air, water, etc.) or dark events due to the detector noise. Therefore, several algorithms have been designed to detect pixel with useful photons, i.e., photons reflected from an object or a surface. Such approaches include the Markov chain Monte-Carlo (MCMC) method proposed in [8], which is time consuming due to the use of a sampling MCMC strategy. Two fast algorithms were recently proposed in [9, 10], which use a Bayesian formulation to output a per-pixel probability of target presence. These algorithms showed state-of-the-art performance, however, they operated on a histogram of counts which is not an optimal data representation given limited computing resources.

This paper proposes a new fast algorithm for per-pixel object detection. We adopt a Bayesian approach operating on the raw ToFs data and defining as parameters the target depth (if present), a signal-to-background related parameter and a binary parameter indicating the presence or absence of a target. A probability mixture model is considered for the likelihood, while appropriate prior distributions are chosen for each model parameters to express their known properties. The resulting model selection problem is then solved by marginalizing the depth and SBR parameters, leading to analytical expressions for the probability of detecting a target. The resulting analytical expressions are however combinatorial, and an approximation is introduced to ensure fast computations. The proposed approach is validated on simulated and real Lidar data showing good performance when compared to the algorithm [9] in terms of computational cost and detection performance.

The paper is structured as follows. Section 2 introduces the observation model of the detected photon events. Section 3 presents the proposed Bayesian model for target detection. The computation of the marginal probabilities are described in Section 4. Results and conclusions are finally reported in Sections 5 and 6.

2. OBSERVATION MODEL

Single-photon Lidar systems generally emit laser pulses and detect the reflected photons, together with their ToFs, from the target for each spatial location/pixel. The detected photons and measured ToFs provide useful information regarding the distance of the observed target and its reflectivity, allowing the construction of 3D images of the observed scene. It is common to gather the measured ToFs into a histogram of counts $y_{n,t}$, for the nth pixel and tth bin where $n \in \{1, \cdots, N\}$ and $t \in \{1, \cdots, T\}$, which is modelled using a Poisson distribution given by

$$y_{n,t} \sim \mathcal{P}\left[r_n\, g\left(t - d_n\right) + b_n\right] \tag{1}$$

where $\mathcal{P}(.)$ denotes a Poisson distribution, $d_n \in \{1, \cdots, T\}$ represent target range's position, $r_n \geq 0$ the reflected counts from the target, $b_n \geq 0$ denotes the background and dark counts of the detector, g is the system impulse response (SIR) assumed to be known from a calibration step and normalized ($\sum_{t=1}^{T} g\left(t\right) = 1$) and T is the length of the ToFs histogram. In the absence of a target, i.e. $r_n = 0$, the measured histogram reduces to background counts $y_{n,t} \sim \mathcal{P}\left(b_n\right)$. In this paper, we approximate the SIR with a Gaussian shape as it helps obtain analytical probability results in Section 4. Model (1) has been used in many studies, however, it assumes the availability of histograms which in practice should be built from the raw detected photons and ToFs and thus involve additional computational cost. In addition, modelling the data using histograms is memory consuming especially in the sparse photon regime where only few photons are detected per-pixel. In this paper, we aim to design a low memory and fast detection algorithm, thus we directly model the detected list of photons $s_{n,m}$ for the nth pixel and for $m \in \{1, \cdots, \bar{y}\}$, using a mixture of densities as in [11, 12]

$$P(s_{n,m}|w_n, d_n) = \frac{(1 - w_n)}{T} + w_n g\left(s_{n,m} - d_n\right) \tag{2}$$

where $w_n = \frac{r_n}{r_n + b_n T}$ represents the probability of the detected photon to belong to a target or a uniform background and $\bar{y}$ the total number of photons detected in the nth pixel. Model (10) shows that in absence of a target in the nth pixel (i.e., $r_n = w_n = 0$), the ToFs will be uniformly distributed as follows

$$P(s_{n,m}|w_n = 0, d_n) = 1/T. \tag{3}$$

Assuming the independence of the observed ToFs leads to the joint likelihood distribution

$$P(\boldsymbol{s}_n|w_n, d_n) = \prod_{m=1}^{\bar{y}} P(s_{n,m}|w_n, d_n). \tag{4}$$

where $\boldsymbol{s}_n = (s_{n,1}, \cdots, s_{n,\bar{y}})$ gathers all detections for the nth pixel. Given a ToFs list denoted by $\boldsymbol{s}_n$, our goal is to design a fast target detection algorithm to decide if $0 < w_n \leq 1$ or $w_n = 0$, i.e, if there is a target or not. Note that this is an ill-posed inverse problem, since the parameters (w_n, d_n) are unknown in practice, and we propose to solve it using a Bayesian strategy as detailed in the next section.

3. BAYESIAN MODEL FOR TARGET DETECTION

This section introduces a Bayesian model for target detection. The Bayesian framework assigns prior distributions to the unknown parameters to include additional information and regularize the ill-posed inverse problem. The next section introduces the proposed prior distributions for the unknown parameters.

3.1. Prior distribution for w

The parameter $0 \leq w_n \leq 1$ represents the probability of the detected ToFs to belong to a background ($w_n = 0$) or a target ($0 < w_n \leq 1$). To satisfy these constraints, we assign this parameter a common spike and slab prior distribution [13] as follows

$$p(w_n|u_n) = \delta(w_n)(1 - u_n) + u_n Beta(\alpha, \beta) \tag{5}$$

where $\delta(.)$ denotes the Dirac delta distribution centred in 0, $Beta(\alpha, \beta)$ is the beta distribution with known shape parameters $\alpha, \beta > 0$ and $u_n \in \{0, 1\}$ is a binary variable that indicates the presence ($u_n = 1$) or absence ($u_n = 0$) of a target. In this work, the parameters $\alpha, \beta > 0$ are assumed known and fixed to reflect our prior knowledge on the parameter w_n. The latter parameter is directly related to the signal to background (SBR) level (as follows $w_n = \frac{\text{SBR}}{1+\text{SBR}}$, where SBR$= r_n/(b_n T)$) which allow fixing the hyper-parameters from calibration measurements. In what follows, we assume non-informative prior and fix the parameters to $\alpha = \beta = 1$.

3.2. Prior distribution for u_n

The parameter u_n is assigned a Bernoulli distribution with a probability of target presence π, i.e., $p(u_n = 1) = \pi$ and $p(u_n = 0) = 1 - \pi$. The parameter π is fixed to 0.5 in what follows, reflecting the absence of additional information regarding this parameter.

3.3. Prior distribution for d_n

A non-informative uniform prior distribution is assigned for the discrete variable d_n, as follows $p(d_n) = 1/T, \forall n$. However, this choice can be changed in presence of additional information regarding the target position.

3.4. Posterior distribution and decision rule

Using Bayes rule, the posterior distribution can be expressed as follows

$$f(w_n, d_n, u_n|\boldsymbol{s}_n) \propto f(\boldsymbol{s}_n|d_n, w_n) f(d_n) f(w_n|u_n) f(u_n) \tag{6}$$

where $\propto$ means "proportional to". To perform target detection, we are interested on the marginals of the variable u_n and

build our test rule as in [9]

$$f(u_n = 0|\boldsymbol{s}_n) \underset{H_1}{\overset{H_0}{\gtrless}} f(u_n = 1|\boldsymbol{s}_n) \tag{7}$$

where H_0, (resp. H_1) represents the absence (resp. presence) of a target and

$$f(u_n|\boldsymbol{s}_n) = \sum_{d_n=1}^{T} \int_0^1 f(w_n, d_n, u_n|\boldsymbol{s}_n) dw_n \tag{8}$$

The next section introduces the details to compute (8)

4. COMPUTATION OF DETECTION PROBABILITIES

Our goal is to compute the marginals in (8). It is straightforward to show that

$$p(u_n = 0|\boldsymbol{s}_n) = \frac{1-\pi}{T^{\bar{y}}}. \tag{9}$$

To compute $p(u_n = 1|\boldsymbol{s}_n)$ we first note that the joint likelihood distribution can be expressed as a polynomial, as follows

$$\begin{aligned} p(\boldsymbol{s}_n|w_n, d_n) &= w_n^{\bar{y}} \prod_{m=1}^{\bar{y}} [x_n + g(s_{n,m} - d_n)] \\ &= w_n^{\bar{y}} \sum_{m=0}^{\bar{y}} a_{nm}(d_n) x_n^m \end{aligned} \tag{10}$$

where $x_n = \frac{(1-w_n)}{Tw_n}$, and $a_{nm}(d_n) > 0$ are expressed with respect to the sum and product of the coefficients $r_m^{d_n} = g(s_{n,m} - d_n)$ using the Vieta's formulas given by

$$a_{nm}(d_n) = \sum_{1 \le i_1 \le i_2 \le \cdots \le i_k \le \bar{y}} r_{i_1}^{d_n} r_{i_2}^{d_n} \ldots r_{i_k}^{d_n} \tag{11}$$

At this stage, we approximate the SIR g (which is playing the role of signal counts distribution) by a Gaussian distribution with standard deviation σ as follows $g(s_{n,m} - d_n) = \mathcal{N}_{d_n}(s_{n,m}, \sigma^2)$. This is a common approximation that has been used in several previous studies [14] [15]. It is worth mentioning that using a continuous Gaussian distribution to represent the discrete ToF values has a limited effect on the performance of the proposed approach, this is due to the time resolution of single-photon detectors being generally very small compared to σ. Under these assumptions, Eq. (11) reduces to a sum and products of Gaussian distributions which is analytically available. The marginalization in (8) can be analytically done leading to

$$\begin{aligned} p(u_n = 1|\boldsymbol{s}_n) = & \frac{\pi}{TBeta(\alpha,\beta)} \\ & \times \sum_{m=0}^{\bar{y}} \left[\frac{Beta(\bar{y}+\alpha-m, \beta+m)}{T^i} \bar{a}_{nm} \right] \end{aligned} \tag{12}$$

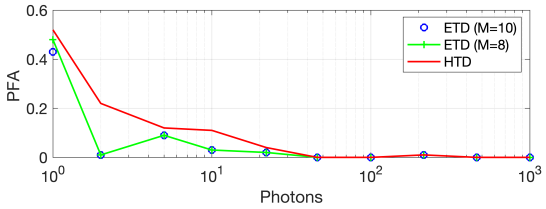

Fig. 1. Comparison of false alarm probability for the proposed method with different approximation levels, and the histogram-based method in [9].

where $\bar{a}_{nm}$ is the result of marginalizing the Gaussians in $a_{nm}(d_n)$ with respect to d_n, where we have assumed the target location d_n is far from the observation window edges leading to $\sum_{d_n} \mathcal{N}_{d_n}(\mu, \sigma^2) \approx 1$. Although Eq. (12) shows an analytical formula for the probability of detection, it should be noted that it is a sum of combinatorial products (see (11)) that can not be computed efficiently for large $\bar{y} > 10$. Several strategies can be adopted to solve this problem and we distinguish two promising directions, (i) an iterative estimation approach where (12) is evaluated for a small number of photons M, the resulting probability is then used to update our prior distribution by setting $\pi_n^{t+1} = p(u_n^t = 1|\boldsymbol{s}_n^t)$. The procedure can be repeated iteratively to account for all detected photons $\bar{y}$. The second strategy, which is adopted in this paper, is to approximate $p(u_n = 1|\boldsymbol{s}_n)$ by limiting the number of terms summed in (11) to $K = \binom{M}{M/2} = \frac{M!}{(M/2)!(M/2)!}$, where M is a user fixed parameter ensuring better approximation for large values and ! denotes the factorial operator. Note that the complexity of the proposed algorithm is proportional to the small number of detected photons instead of the size of observation window "T" as in [9].

Finally we mention that the obtained probability maps results from an independent processing of pixels. Assuming a similar number of surfaces for adjacent pixels [9, 16], the probability maps can be post-processed to enforce spatial correlation between pixels using a total-variation regularization as in [9]. The latter procedure leads to better visual results as shown in the next section.

5. RESULTS

We first evaluate the performance of the proposed algorithm, denoted ETD for event based target detection, on simulated data. We generate the data according to model (10) with $T = 2500$bins, $\sigma = 20$, while varying SBR in the range $[0.01, 100]$ and the total photons $\bar{y}$ in the range $[1, 1000]$. The proposed strategy is evaluated for two approximation levels $M \in \{8, 10\}$ and is compared to the histogram based TD algorithm (HTD) introduced in [9] as it showed state-of-the-art results with reduced computational time. All results are

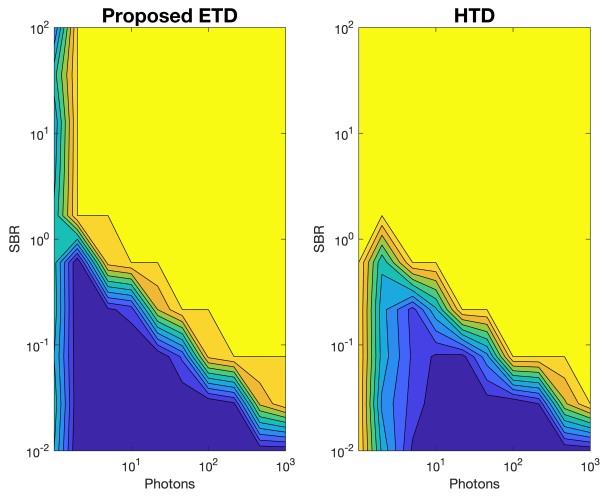

Fig. 2. Comparison of true positive (TP) probability for (left) the proposed method with M=10 and (right) the histogram-based method in [9]).

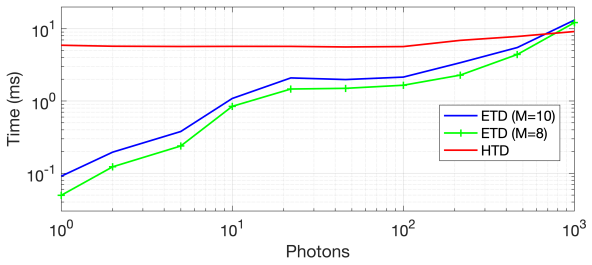

Fig. 3. Comparison of the computational time of the proposed method with different approximation levels, and the histogram-based method in [9].

obtained on Matlab 2018a on a Mac Quad-Core Intel Core i7@3.1GHz, 16 GB RAM. Fig. 1 shows the probability of false alarm (PFA) of the two algorithms highlighting the good results of the proposed strategy. The true positive (TP) probabilities are presented in Fig. 4 where the algorithm [9] shows more detection for low photons leading to better TP at the expense of a higher PFA. The main benefit of the proposed algorithm is the reduced computational time of the order of 1ms per-pixel for M=10, as illustrated in Fig. 3, which shows an improvement factor of 10 compared to the algorithm [9]. Fig. 3 shows however that the proposed algorithm complexity is proportional to the approximation coefficient M, and to the number of detected photons, showing best performance for $\bar{y} < 100$ per pixel.

The proposed strategy is also validated on real data. Akin to [9], we consider the mannequin face scene measured at a stand-off distance of 325 metres at midday in Heriot-Watt

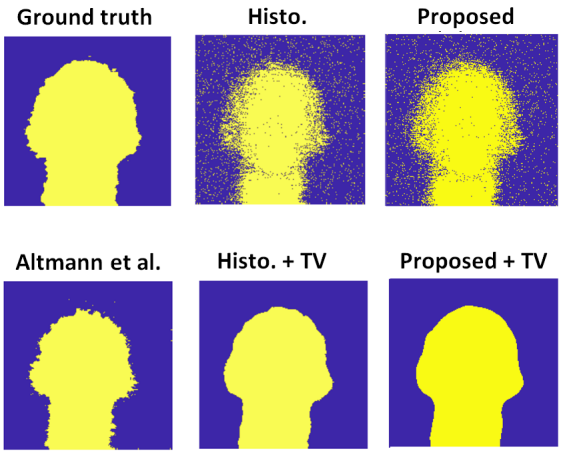

Fig. 4. Detected maps for the mannequin face with 3ms acquisition time per pixel (yelow: a detected target, blue: no target).

University, in bright conditions. The data has 200x200 pixels, T=1700 bins, an SBR of 0.29 with a 5th-95th percentile interval of (0.05,0.67). We focus on the data with 3ms acquisition time per pixel which has 61 average photon-per-pixel, and we refer the reader to [8,9] for more details regarding this dataset. Results in Table 1 shows the PD, PFA and computational cost of the studied methods (when enforced, spatial regularization is denoted by TV) showing good performance for the proposed strategy (for M=10) especially in term of computational cost. Fig. 4 shows the obtained detection maps with ETD, HTD [9] and Altmann et al[8] indicating similar performance, before and after applying spatial regularization.

Table 1. Probability of detection (PD), false alarm (PFA) and computational times (in ms) of the two methods on real data with different acquisition times. The processing time is indicated in ms for each pixel while assuming a parallel processing. The TV regularization requires 31ms for the full image.

		HTD	HTD-TV	ETD	ETD-TV
3ms data	PD(%)	80	92	85	93
	PFA(%)	4	0.07	6	0.11
	Time (ms)	6	6+ 31 (TV)	1	1+ 31 (TV)

6. CONCLUSIONS

This paper has introduced a new algorithm for fast target detection in single-photon Lidar data. In contrast to histogram based methods, the proposed strategy operates on single-photon ToF events to reduce memory requirements and ensure fast processing. The proposed algorithm showed good

performance especially in presence of few photons per pixel, which is a common scenario for rapid or long-range imaging. The algorithm can serve as a building block for higher-level applications such as adaptive sampling to improve data acquisition [17], and can be used as a pre-processing step to several reconstruction algorithms [11, 14, 18–21]. Future work includes the consideration of a different approach to enforce spatial regularization between pixels. Considering an iterative approach to approximate the marginal posterior is also interesting for the fast online processing of the detected photons. A generalization to imaging through obscurants will also be investigated.

7. ACKNOWLEDGMENT

The authors thanks Dr. Tachella for sharing the HTD code used for comparison in this work.

8. REFERENCES

[1] A. M. Wallace, A. Halimi, and G. S. Buller, "Full waveform lidar for adverse weather conditions," *IEEE Trans. Vehicular Tech.*, 2020, In press.

[2] A. M. Wallace, A. McCarthy, C. J. Nichol, X. Ren, S. Morak, D. Martinez-Ramirez, I. H. Woodhouse, and G. S. Buller, "Design and evaluation of multispectral lidar for the recovery of arboreal parameters," *IEEE Trans. Geosci. Remote Sens.*, vol. 52, no. 8, pp. 4942–4954, 2014.

[3] A. M. Pawlikowska, A. Halimi, R. A. Lamb, and G. S. Buller, "Single-photon three-dimensional imaging at up to 10 kilometers range," *Opt. Express*, vol. 25, no. 10, pp. 11 919–11 931, May 2017.

[4] G. Satat, M. Tancik, and R. Raskar, "Towards photography through realistic fog," in *Computational Photography (ICCP), 2018 IEEE International Conference on*. IEEE, 2018, pp. 1–10.

[5] A. Halimi, A. Maccarone, A. McCarthy, S. McLaughlin, and G. S. Buller, "Object depth profile and reflectivity restoration from sparse single-photon data acquired in underwater environments," *IEEE Trans. Comput. Imaging*, vol. 3, no. 3, pp. 472–484, 2017.

[6] A. Maccarone, A. McCarthy, X. Ren, R. E. Warburton, A. M. Wallace, J. Moffat, Y. Petillot, and G. S. Buller, "Underwater depth imaging using time-correlated single-photon counting," *Opt. Express*, vol. 23, no. 26, pp. 33 911–33 926, Dec 2015.

[7] R. Tobin, A. Halimi, A. McCarthy, M. Laurenzis, F. Christnacher, and G. S. Buller, "Three-dimensional single-photon imaging through obscurants," *Opt. Express*, vol. 27, no. 4, pp. 4590–4611, Feb 2019.

[8] Y. Altmann, X. Ren, A. McCarthy, G. S. Buller, and S. McLaughlin, "Robust bayesian target detection algorithm for depth imaging from sparse single-photon data," *IEEE Trans. Comput. Imaging*, vol. 2, no. 4, pp. 456–467, 2016.

[9] J. Tachella, Y. Altmann, S. McLaughlin, and J. . Tourneret, "Fast surface detection in single-photon lidar waveforms," in *EUSIPCO-19*, A Coruna, Spain, 2019, pp. 1–5.

[10] J. Tachella, Y. Altmann, S. McLaughlin, and J.-Y. Tourneret, "On fast object detection using single-photon lidar data," in *Wavelets and Sparsity XVIII*, vol. 11138. SPIE, 2019, pp. 252 – 261.

[11] J. Rapp and V. K. Goyal, "A few photons among many: Unmixing signal and noise for photon-efficient active imaging," *IEEE Trans. Comput. Imaging*, vol. 3, no. 3, pp. 445–459, Sept. 2017.

[12] Y. Altmann and S. McLaughlin, "Range estimation from single-photon lidar data using a stochastic em approach," in *EUSIPCO-18*, Rome, Italy, Sept. 2018, pp. 1112–1116.

[13] E. I. George and R. E. McCulloch, "Variable selection via gibbs sampling," *Journal of the American Statistical Association*, vol. 88, no. 423, pp. 881–889, 1993.

[14] A. Halimi, Y. Altmann, A. McCarthy, X. Ren, R. Tobin, G. S. Buller, and S. McLaughlin, "Restoration of intensity and depth images constructed using sparse single-photon data," in *Proc. EUSIPCO*, 2016, pp. 86–90.

[15] Y. Altmann, S. McLaughlin, and M. E. Davies, "Fast online 3d reconstruction of dynamic scenes from individual single-photon detection events," *IEEE Transactions on Image Processing*, vol. 29, pp. 2666–2675, 2020.

[16] S. Hernandez-Marin, A. M. Wallace, and G. J. Gibson, "Multilayered 3D lidar image construction using spatial models in a bayesian framework," *IEEE Trans. Pattern Anal. Mach. Intell.*, vol. 30, no. 6, pp. 1028–1040, June 2008.

[17] A. Halimi, P. Ciuciu, S. McLaughlin, and G. S. Buller, "Fast adaptive scene sampling for single-photon 3d lidar images," in *IEEE International Workshop on Computational Advances in Multi-Sensor Adaptive Processing (CAMSAP)*, Guadeloupe, France, Dec 2019.

[18] J. Tachella, Y. Altmann, X. Ren, A. McCarthy, G. S. Buller, S. McLaughlin, and J.-Y. Tourneret, "Bayesian 3d reconstruction of complex scenes from single-photon lidar data," *SIAM Journal on Imaging Sciences*, vol. 12, no. 1, pp. 521–550, 2019.

[19] A. Halimi, R. Tobin, A. McCarthy, J. Bioucas-Dias, S. McLaughlin, and G. S. Buller, "Robust restoration of sparse multidimensional single-photon lidar images," *IEEE Trans. Comput. Imaging*, vol. 6, pp. 138–152, 2020.

[20] D. Shin, F. Xu, F. N. C. Wong, J. H. Shapiro, and V. K. Goyal, "Computational multi-depth single-photon imaging," *Opt. Express*, vol. 24, no. 3, pp. 1873–1888, Feb 2016.

[21] R. Tobin, A. Halimi, A. McCarthy, X. Ren, K. J. McEwan, S. McLaughlin, and G. S. Buller, "Long-range depth profiling of camouflaged targets using single-photon detection," *Optical Engineering*, vol. 57, pp. 031 303 (1–10), 2017.